Proceedings of the International Computing and Communication Conference (I3C 2024)

https://i3c.futminna.edu.ng/ www.futminna.edu.ng https://www.ncc.gov.ng/

A Pattern Reconfigurable Metamaterial-Based Antenna for Sub-6G Millimeter-Wave Application

Lawal Abubakar[1*], Nathaniel Salawu[2], Salihu Alhaji Bala[3], Sunday Achimugu[4]
[1]Shiroro Hydroelectric Power Station, Shiroro, Niger State
[2, 3,4]Federal University of Technology Minna
[*]lawalabubakar70@gmail.com, +2348033717757

ABSTRACT
The increasing number of applications, services, and use case scenarios triggers the evolution from the fifth generation (5G) towards the sixth generation (6G). 6G has been envisioned to utilize the sub-THz (90-300 GHz) (upper mmWave) and THz (0.1-10 THz) bands. At such high frequencies, high path loss and atmospheric absorption are critical challenges. A highly directional and reconfigurable antenna is required to mitigate these challenges. In this paper, a novel pattern reconfigurable metamaterial-based antenna for sub-mmWave applications is proposed. The antenna is based on a graphene metasurface loaded with a novel square-spherical split ring (SSSR) resonator, placed above a rectangular microstrip patch antenna to provide absorption of unwanted signal and improve gain and spectral efficiency. Placed under the patch is Rogers 5800 substrate with permittivity (ε) of 2.0 and thickness of 0.1mm. The antenna operates between 90-120 GHz spanning the 102-109 GHz adopted at the WRC 2023 for advanced use cases of 6G and was simulated using CST suite. The main beam is pattern reconfigured by two PIN diodes (d_1, d_2) embedded on the patch antenna. d_1 switches between 90-98 GHz, obtaining a maximum radiation pattern of -70.7 dB at 97.5GHz, while d_2 switches between 98 -120GHz, realizing a -69.6dB peak radiation pattern at 105.4GHz. When fully loaded, a -64.5dB was obtained, better than similar work compared. The antenna is compact, has a wide bandwidth, and can perform efficiently in 6G use cases such as holographic presence, and smart transport among others requiring high radiation efficiency.

Keywords: *antenna, 6G, metamaterial, reconfigurable, mmWave*

1. INTRODUCTION

Wireless communication has evolved from the conventional analogue telephone system to broadband interconnection that we have today. It is anticipated that more than 90 billion gadgets will have wireless connectivity by 2030. (Shahraki et al., 2021). New use cases such as holographic presence, tactile internet, ubiquitous connectivity, and extremely high-definition video are anticipated. The existing generation of wireless communication technologies including 5G will not be able to handle the current surge in data traffic and the new applications as depicted in Figure 1. Sixth-generation (6G) networks are being launched as the next generation of wireless providing ultra-high reliable data speed at extremely low latency, high efficiency, and ubiquitous connectivity (Wang et al., 2023).

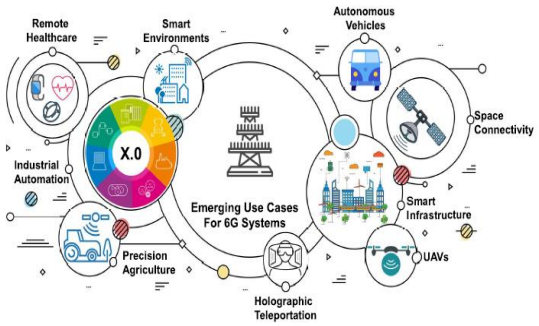

Fig.1: New application use cases of 6G (Wang et al. 2023)

Due to the overwhelming demand for higher data rates, 5G technology is currently being upgraded to 6G communication systems, which prioritize ultra-low latency, ultra-large bandwidth, ultra-high

capacity, ultra-high security, and ubiquitous connectivity (Bang et al. 2023). This has resulted in a persistent demand for higher data capacity, which calls for additional bandwidth and spectrum. (Andersson et al. 2023). To deliver ultra-high capacity, emerging 6G technology will rely on new air interface (reconfigurable intelligent surface (RIS) and massive-multiple-input-multiple-output (mMIMO)) (Roy and Dhillon 2021), ultra-large bandwidth will be catered by new spectrum (mmWave, THz, and visible light communication(VLC)) (Pant and Malviya 2023), (Al-kinani et al. 2023). Ubiquitous connectivity will be achieved by integrated space and terrestrial network (ISTN) (Ziegler et al. 2020), while Artificial Intelligence, Blockchain technology, and quantum communication will be utilized by 6G to provide ultra-secured and reliable connection (Bang et al. 2023).

As the demand for seamless connectivity grows, there arises a need for antennas (which refer to structures within the region of transmission between a guided wave and free space that intercept and propagate electromagnetic wave and vice versa (Achimugu et al. 2023)) that can effectively operate across these frequency bands. Over time, cellular and Wi-Fi systems have steadily shifted from using basic patch and monopole antennas to more sophisticated beamforming array antennas, which are employed in the most recent 4G and 5G generations of wireless technology in multiple-input multiple-output (MIMO) systems (Olwal, and Lysko 2021).

In 5G mobile communication system, the lower mm-Wave band (<90GHz) is sufficient to deliver 10Gbps data rate (Vyas 2019). For such band, multiple-input-multiple-output (MIMO) antenna configurations are been widely implemented. The authors in (Griffiths et al. 2023) presented a mm-wave antenna design using a ring-slot resonator to achieve a wide bandwidth of 25.0-29.7 GHz. Even though MIMO antennas produce good spatial radiation, coupling between the ports is a drawback as reduces the antenna performance. Efficient isolation in MIMO antennas can be attained by the application of metamaterial-based MIMO design techniques. (You et al., 2022.).

Future 6G networks have been envisioned to utilize upper mmWave, THz, and VLC bands (Kumar and Chavhan 2022). Despite the promising results of mmWave communication systems, it suffers from high signal attenuation, absorption, and penetration loss. Developing workable solutions for high-mobility contexts, enhancing the reach of communications, reducing hardware impairments, overcoming sensitivity to blockages, and atmospheric loss are open research directions in mmWave for 6G (Ichkov, and Simić 2023).

THz communication might potentially offer greater bandwidth than mmWave frequency and better propagation conditions, however, the design challenges at such very frequency have limited researchers. For the 6G network, operating at higher frequency ranges made possible by THz communications may be effectively utilized to enable a variety of distant sensing applications. Furthermore, the Internet of NanoThings (IoNT) and the Internet of BioNanoThings (IoBT) are two examples of future emergent micro-scale applications that THz communications can support efficiently (Akyildiz, and Nie 2020). While the mmWave and THz spectrum have been widely envisioned for 6G, ITU-R at the WRC 2023, harmonized frequency bands for the development of next-generation mobile communication (Castro 2023) within the mmWave spectrum. as shown in Table I. (Castro 2023). This paper focuses on the design of an antenna for the advanced use cases spectrum of 6G. In this paper, a

novel SSSR pattern reconfigurable metamaterial antenna operating between 90 – 120GHz has been designed using the CST suite. The performance of the antenna has been compared with similar structures for 6G and shows better performance. The antenna is aimed at achieving spectral efficiency in 6G thereby reducing the signal path loss through self-reconfiguration in the direction of available signal power. The remainder of this paper is arranged as follows.

Table I. Adopted Spectrum for 6G Development by ITU-R at WRC 2023

Adopted 6G Spectrum	
Mobile communication	**All region:** 6425MHz – 7125MHz **Region 1:** 4400-4800MHz, 7125-7250MHz, 7750-8400MHz, 14.80-15.35GHz **Region 2:** 7125-8400MHz, 14.80-15.35GHz **Region 3:** 4400-4800MHz, 7125-8400MHz, 14.80-15.35GHz
Advanced use cases	102-109 GHz, 167-174 GHz, 151.5-164 GHz, 209-226 GHz, 252-275 GHz

2. RELATED WORKS

Antennas for 6G networks are expected to resonate at high frequency, be highly directional, reconfigurable, and operate at wide bandwidth (Nor et al., 2020). Antenna reconfigurations are classified according to frequency, pattern, polarization, or hybrid and can be achieved by using PIN diodes, Microelectromechanical systems (MEMS), tunable varactors, optical devices, or mechanical techniques (Mallik et al., 2022). In this paper, we leverage the metasurface capability to tune its radiation pattern in to achieve pattern reconfigurability with the aid of PIN diodes.

The challenge of high path loss and atmospheric absorption at mmWave has led researchers to design different antenna structures to mitigate the losses. The authors in (Sheriff et al. 2022), proposed a graphene plasmonic two-port Terahertz (THz) MIMO antenna based on a Teflon substrate of 130 × 85 µm2 was proposed. The antenna delivered a wide impedance bandwidth of 0.6 THz, low envelope correlation coefficient (ECC) of 0.000168, compact size, stable radiation, high gain of 7.23 dB, and low channel capacity loss (CCL) of 0.006. In a similar work, (Wong, and Li 2023) proposed a 2 × 2 module array with 16 ports that are closely placed and made up of four low-profile MIMO antenna modules on a 0.4-mm thick FR4 substrate. The antenna operates within 7.025-8.4 GHz. They fabricated into a 16 × 8 MIMO to achieve a high spectral efficiency of about 56 bps/Hz.

In the quest to deliver high gain, a tooth-shaped inset-fed patch antenna based on Rodgers 5880 substrate that operates at the sub-THz band with a center frequency of 0.19THz was designed by (Vyas and Mohammad 2020). The antenna has a gain of 9.58dB and a return loss of -47.71 dB. Similarly, a compact coplanar waveguide (CPW) fed ultra-wideband (UWB) microstrip patch antenna based on Rodgers 5880 substrate, operating between 23–150 GHz was designed by (Omi et al. 2023) and simulated in ANSYS HFSS. The antenna gain recorded a 14.8 dB

gain at 90 GHz. (Md Hedayatullah et al. 2022) in their work presented a wideband aperture-coupled patch antenna for sub 6G THz band. A peak gain of 7.95dBi and $S_{11} \leq$ -10dB was achieved across a wide frequency range of 90 – 128.5GHz.

In the work by (Nissanov and Singh 2021), a reconfigurable mmWave/THz microstrip antenna for ultra-wideband (UWB) was proposed, featuring two PIN diodes mounted on a benzocyclobutene (BCB) polymer and a gold radiating patch. For the ON and OFF states of the PIN diodes utilized, the equivalent resistor (R), capacitor (C), and inductor (L) were, respectively, 100 pH, 4 fF, and 10 ohms. The antenna operated between 100GHz-303 GHz utilizing frequency reconfiguration to obtain a maximum gain of 8.59 dB at 201.77 GHz and was simulated using CST MWS. Similarly, a photonic-controlled reconfigurable antenna was proposed by (Muqdad et al. 2023). The antenna operates across 0.978 GHz to 1.73 GHz with S_{11} better than −10 dB and a gain of 9 dBi at 1.35 GHz. The suggested antenna is made up of a regular rectangular patch with an order 3 H-tree fractal slot incorporated in it. The patch radiator is positioned above a metasurface layer that has a small air gap between it and the radiator. The metasurface layer is made of a lattice structure of unit cells coupled to one another by PIN photodiodes, which allow the antenna to be reconfigured.

In preparation for the 6G era, the sub-THz band and THz bands have witnessed the use of metasurface antenna made up of periodic square split-ring resonators (SRRs). SSRs consist of an inductive line and a capacitive gap to achieve magnetic and electric coupling and influence the antenna radiation pattern (Mishra, and Pahadsingh 2022). Aside from path loss and unprecedented absorption faced with sub-mmWave and THz, the changing position of devices will be another challenge. Novel techniques that provide full antenna beam coverage and stable radiation patterns with higher directive gain are needed to focus the radiation pattern in the direction of the device.

3. METHODOLOGY

3.1. Metamaterial Selection

Metamaterials (MMs) are characterized by effective permittivity (ε) and permeability (μ). Let the effective permittivity, permeability, and refractive index be denoted as ε_e , μ_e, n_e.

The effective refractive index of metamaterials is given by (1) (Hussain et al. 2023).

$$n_e = \sqrt{\mu_e} \cdot \sqrt{\varepsilon_e} \quad (1)$$

When electromagnetic wave hits the MM, the permeability becomes (2).

$$\mu_e = 1 - \frac{F}{1 - \frac{2\sigma i}{\omega R \mu_0 (N-1)} - \frac{dC_0^2}{2\pi^2 \omega^2 R^3 (N-1)}} \quad (2)$$

Where; C_0 represent light speed in a vacuum, ω is angular oscillation, σ is the metal conductivity. μ_0 is the permeability of the vacuum, while *F* represents the volume of the structure.

The permittivity is derived from (1) and (2) as in (3)

$$\varepsilon_e = 1 - \frac{\omega_{pe}^2}{\omega^2 + i\omega\omega_c} \quad (3)$$

$$\omega_{pe}^2 = \frac{\rho e^2}{\epsilon_0 m_e} \quad (4)$$

Note that, ω_{pe} is the frequency of electric plasma, ω_c is the collision pulse, and ρ is the electrons' density. The electron charge is e and m_e represent the effective mass of the electrons. MMs that have negative (ε) and positive (μ) or vice versa are preferred for application at high frequencies while those with near DNG are preferred for THz and beyond. When materials that have negative ε and positive (μ) or vice versa are exposed to an incident wave coming from an

electromagnetic source, they distribute the electric and magnetic wave in equal azimuthal direction efficiently. A material that exhibit this property is graphene. This substantiates the selection of graphene for this work.

3.2. Antenna Geometry and Design

The proposed antenna geometry is shown in Figure 2. while Table II shows the design parameters. The structure is based on a graphene metasurface placed above the patch antenna to provide absorption of unwanted signal, and improve gain and spectral efficiency. The main beam is reconfigured by PIN diodes embedded on the microstrip antenna. Placed under the patch is Rogers 5800 substrate with permittivity (ε) of 2.0 and thickness of 0.1mm and a reflective annealed that enhances the antenna's front-to-back ratio by blocking radiation coming from the patch's backside. Beam steering is achieved by the metasurface layer loaded with unit cells as shown in Figure 3. The metasurface allows maximum radiation pattern on the antenna to enable optical switching of the embedded PIN diodes on the antenna, leading to pattern reconfiguration of the antenna. The gap between the metasurface, patch, substrate, and the annealed reflecting copper is carefully chosen as 0.01mm to prevent complete internal reflection at the wave incidence's crucial angle. Excitation of the patch antenna occurs via a 50 Ω microstrip feedline.

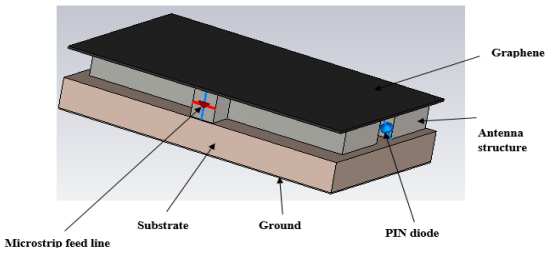

Fig 2: Proposed structural design of 6G reconfigurable antenna

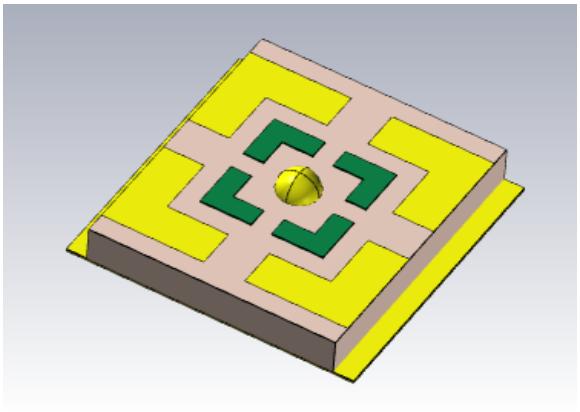

Fig 3: Metamaterial SSSR Unit Cell

Table II: Proposed Antenna Design Parameters

SYMBOL	VALUE (mm)	PARAMETER
L	0.6	Length of the patch
W	1.11	Width of the patch
f_g	0.10	Feed line gap
t_s	0.05	Thickness of the substrate
L	0.8	Length of unit cell
W	0.8	Width of the unit cell
t_g	0.8	Ground thickness
r_{c1}	0.2	Outer square ring cut
r_{c2}	0.08	Inner square ring cut
c_t	0.02	Thickness of the spherical ring
R	0.6	Radius of spherical ring

The antenna structure is made of a rectangular microstrip patch as shown in Fig. 4. PIN diode d_1 and d_2 perform pattern reconfiguration of the beam incident on the metasurface. The two diodes (d_1, d_2) employed in this design are BAR50-02L. According to the datasheet, the diode is equivalent to a series RLC (R = 4Ω, L=C=0) for the ON state and a parallel RLC (R= 5 kΩ, L = 0, C = 0.07 pF) for the OFF state. The antenna is pattern reconfigured by the radiation pattern of the metasurface layer. The dimensions of the rectangular patch antenna are obtained from (Muqdad et al. 2023) as follows;

The length of a rectangular microstrip antenna is given by (5)

$$L = \frac{\lambda_0}{2\sqrt{\varepsilon_e}} - \Delta l \quad (5)$$

The width of the patch is obtained from equation (6)

$$W = \frac{c}{2f_r}\left(\frac{1}{\sqrt{\left(\frac{\varepsilon_r+1}{2}\right)}}\right) \quad (6)$$

The effective permittivity ε_e is derived from (5) and (6) to obtain (7) Type equation here.

$$\varepsilon_e = \frac{e_r+1}{2} + \frac{e_r-1}{2}\left\{\frac{1}{\sqrt{1+\frac{12h}{W}}}\right\} \quad (7)$$

The extension of length of the patch is given by,

$$\Delta l = 0.412h\left(\frac{\varepsilon_e+0.3}{\varepsilon_e-0.258}\right)\left(\frac{(W/h)+0.264}{(W/h)+0.8}\right) \quad (8)$$

Where, λ_0 is the wavelength of the antenna's resonant frequency f_r, Δl is the extension of length of the patch. ε_r denote the permittivity of substrate material and c represent the speed of light in a vacuum.

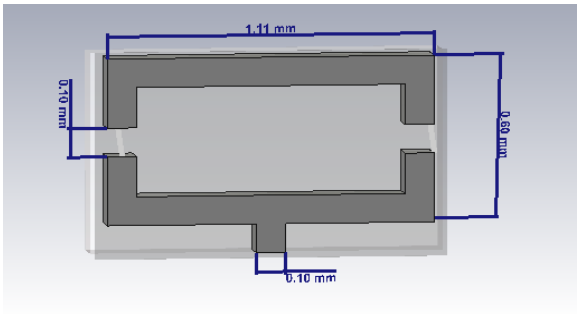

Fig 4: Rectangular patch

4. RESULTS AND DISCUSSION

The structure of the unit cell of a metamaterial determines its performance. While the square split ring (SSR) has been widely adopted in literature, we have developed a novel square-spherical split ring (SSSR) unit cell that achieved less than -10dBi reflection coefficient as shown in Fig. 7, better than the -5dBi obtained by (Omi et al. 2023) which deployed SSR unit cell. The antenna exhibits peak radiation at 118 GHz.

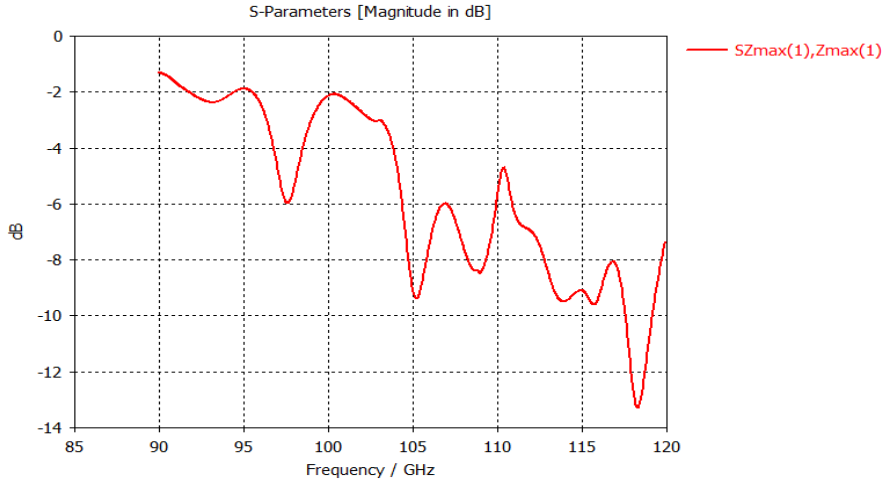

Fig 5: S_{11} plot of SSSR Metamaterial unit cell

The frequency bands of 90-95GHz and 102-120 GHz, show (NZR-ENG) metamaterial properties in the suggested metamaterial structure for the x- and y-directions, respectively. To enable pattern reconfiguration and beam steering, a metamaterial cell must have a near-zero refractive index. As can be seen from Figure 6, the antenna metasurface exhibits near-zero refractive index characteristics.

The PIN diodes are energized by the metal plate of the patch antenna according to the current distribution on the metasurface. The PIN diode d_1 switches at a frequency between 90-98 GHz to the maximum radiation pattern of the antenna which is obtained at 97.5GH as shown in Figure 6.

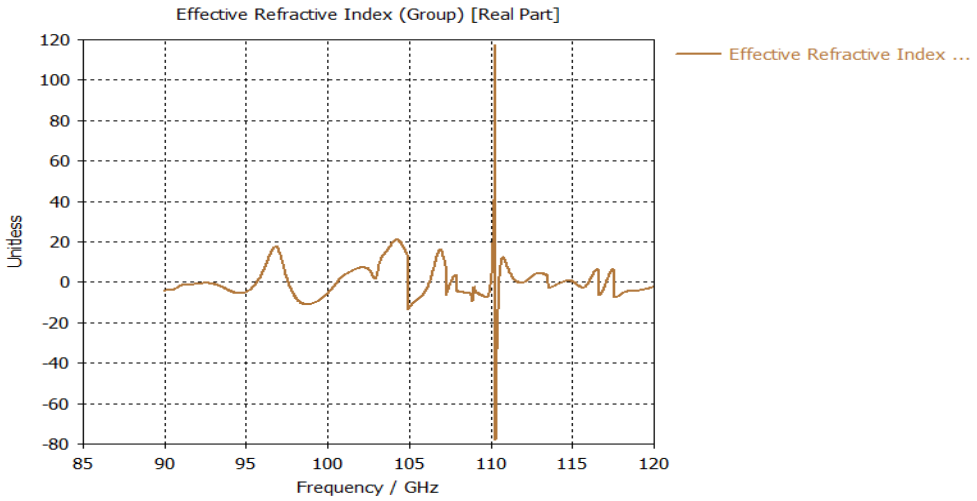

Fig 6: Effective refractive index of the antenna

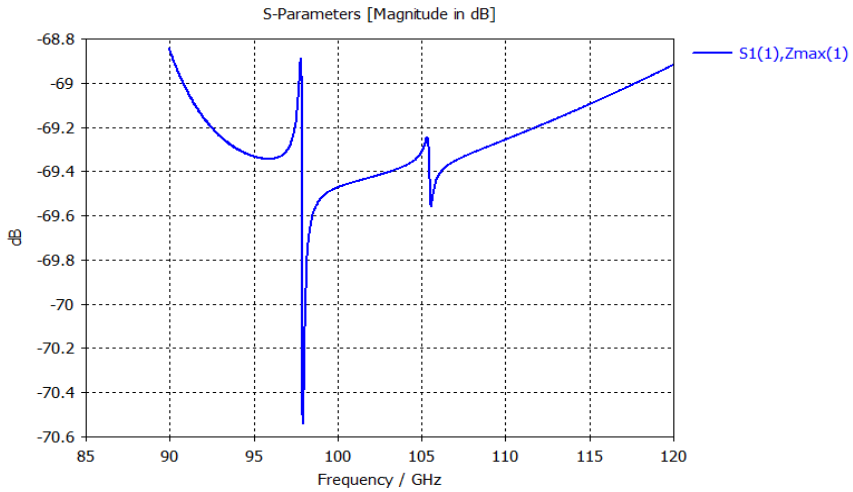

Fig 7: S_{11} of the antenna with metasurface

Figure 8 displays the comparison of the reflection coefficient of the full antenna operation (FS), and when the metasurface was loaded with the unit cells

(SSSR1 and SSSR2). A reflection coefficient, S_{11} of -59.96 dB was realized at 101.2 GHz with a single SSSR unit cell on the metasurface. Only d_1 was ON. Loading the antenna with an array of unit cells (SSSR2) on the metasurface further increases S_{11} by 4% at 101.21GHz, with improved radiation efficiency. Only d_2 was ON. The antenna realized a maximum performance when the two PIN diodes, d_1 and d_2 were ON. S_{11} of –64.5dB. Clearly, the SSSR unit cells drastically increased the performance of the antenna.

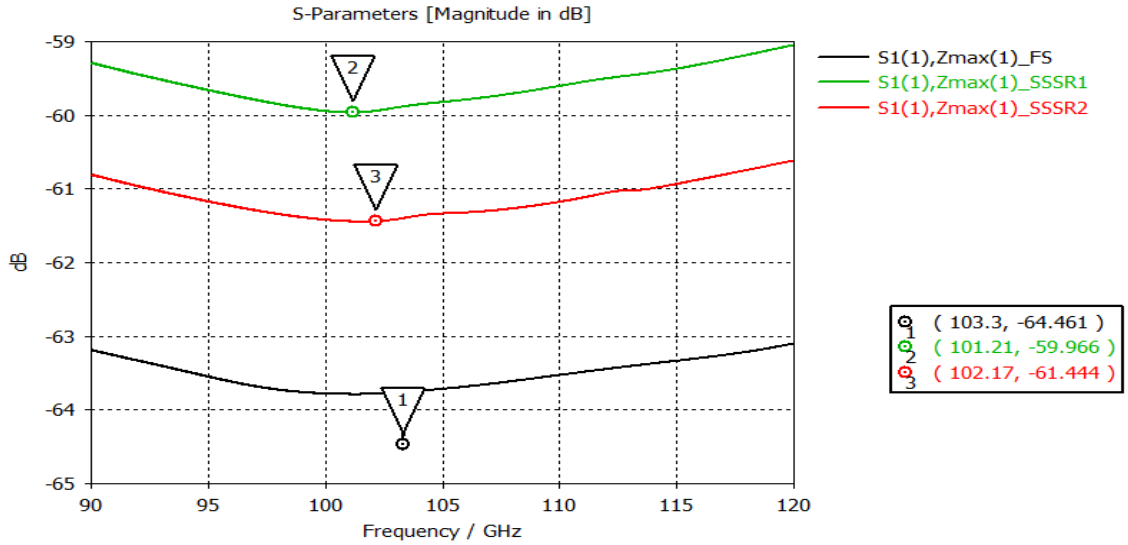

Fig 8: S_{11} of the antenna with SSSR-loaded metasurface

A comparison of the antenna presented in this paper and other state-of-art work is presented in Table III. It can seen that the paper presented in this paper offers a better performance in terms of the reflection coefficient. This is attributed to the novel SSSR unit cell that we proposed as compared to the widely adopted RSS unit cell in literature.

Table III: A comparison of the proposed antenna with related work

Recent work	Frequency (GHz)	Mechanism	Reconfiguration	Bandwidth (GHz)	Reflection coefficient (dB)
(G. Mishra et al., 2022)	2-12	PIN diode	Frequency	10	-28
(Abdulhussein et al., 2023)	2.7-4.8	PIN diode	Frequency	2.1	-32.33
(Sayem et al., 2023)	77	PIN diode	-	-	-42.2
(Muqdad et al., 2023)	0.98-1.73	PIN diode	Frequency	0.75	-25
(M. E. L. Ghzaoui et al., 2023)	180-280	PIN diode	Frequency	100	-55
This paper	**90-120**	**PIN diode**	**Pattern**	**30**	**-64.5**

5. CONCLUSION

In this paper, a novel pattern reconfigurable antenna for 6G advanced use cases has been presented. The antenna is loaded with a novel square split spherical ring unit cell resonator on a graphene metasurface with -1.1 permittivity. The antenna is compact and has a thin structure of $1.2 \times 0.8 \times 0.1$ mm^3. In comparison with other work, the antenna realized a reflection coefficient (S_{11}<<-10) of -64.5dB and 92% radiation efficiency.

REFERENCE

Achimugu, Sunday, Abraham Usman Usman, Lukman Adewale Ajao, and Achonu Adejoh. 2023. "An Optimized Half Wave Dipole Antenna for the Transmission of WiFi and Broadband Networks." *IEEE International Conference on Advanced Innovations in Smart Cities* 1(2):866–68.

Akyildiz, Ian F., Ahan Kak, and Shuai Nie. 2020. "6G and Beyond: The Future of Wireless Communications Systems." *IEEE Access* 8:133995–30. doi: 10.1109/ACCESS.2020.3010896.

Al-kinani, Ahmed, Cheng-xiang Wang, Li Zhou, and Wensheng Zhang. 2023. "Optical Wireless Communication Channel Measurements and Models." *IEEE Communications Survey and Tutorials* 20(3):1939–62.

Andersson, Ingmar, Lars Manholm, Astrid Algaba Brazalez, and Parisa Aghdam. 2023. "Antenna System Requirements and Challenges Towards 6G - An Industrial View." *2023 International Workshop on Antenna Technology, IWAT 2023*(May):610.doi:10.1109/iWAT57058.2023.10171734.

Bang, Ankur, Kapil Kant, Padmaja Joshi, and Kavita Bhatia. 2023. "ScienceDirect 6G : The Next Giant Leap for AI and ML 6G : The Next Giant Leap for AI and ML." *Procedia Computer Science* 218:310–17. doi: 10.1016/j.procs.2023.01.013.

Castro, Caio. 2023. "ITU Defines Frequency Bands for 6G Studies." Retrieved December 18, 2023 (https://www.6gworld.com/exclusives/itu-defines-frequency-bands-for-6g-studies).

Dhinesh Kumar, and Suresh Chavhan. 2022. "Shift to 6G: Exploration on Trends, Vision, Requirements, Technologies, Research, and Standardization Efforts." *Sustainable Energy Technologies and Assessments* 54:102666. doi: https://doi.org/10.1016/j.seta.2022.102666.
Roy, Abhishek, and Harpreet S. Dhillon. 2021. *6G Mobile Wireless Networks*. Springer.

Griffiths, Gabriela Jana, Shaker Alkaraki, Muhammad Aslam, Qammer H. Abbasi, Andrew Evans, and Syeda Fizzah Jilani. 2023. "Millimeter-Wave Defected Ground Structure-Based MIMO Antenna for 6G Wireless Applications." *IEEE Antennas and Propagation Society, AP-S International Symposium (Digest)* 2023-July(July):1399–1400. doi: 10.1109/USNC-URSI52151.2023.10238146.

Hussain, Musa, Wahaj Abbas Awan, Mohammed S. Alzaidi, Niamat Hussain, Esraa Mousa Ali, and Francisco Falcone. 2023. "Metamaterials and Their Application in the Performance Enhancement of Reconfigurable Antennas : A Review." *Micromachines* 14(349):1–26.

Ichkov, A., P. Mähönen, and L. Simić. 2023. "Interference-Aware User Association and Beam Pair Link Allocation in Mm-Wave Cellular Networks." Pp. 1–7 in *2023 IEEE Wireless Communications and Networking Conference (WCNC)*.

Md Hedayatullah, Maktoomi, Wang Zisong, Wang Huan, Saadat Soheil, Heydari Payam, and Aghasi Hamidreza. 2022. "A Sub-Terahertz Wideband Stacked-Patch Antenna on a Flexible Printed Circuit for 6G Applications." *IEEE Transactions on Antennas and Propagation* 70(11):10047–61.

Mishra, Gangadhar, Upali Aparajita Dash, and Sasmita Pahadsingh. 2022. "A Compact Frequency Reconfigurable Antenna Using RSRR for Cognitive Radio Applications." (February). doi: 10.1109/MAPCON56011.2022.10047302.

Muqdad, Zainab S., Mohammad Alibakhshikenari, Taha A. Elwi, Zaid A. Abdul, Bal S. Virdee, Richa Sharma, Salahuddin Khan, Nurhan Türker, Patrizia Livreri,

Francisco Falcone, and Ernesto Limiti. 2023. "Photonic Controlled Metasurface for Intelligent Antenna Beam Steering Applications Including 6G Mobile Communication Systems." *AEUE-International Journal of Electronics and Communications* 166:154–66. doi: 10.1016/j.aeue.2023.154652.

Nissanov, Uri, and Ghanshyam Singh. 2021. "MmWave / THz Reconfigurable Ultra-Wideband (UWB) Microstrip Antenna." (February).

Olwal, Thomas O., Peter Nnabugwu Chuku, and Albert A. Lysko. 2021. "Antenna Research Directions for 6G." 1582–87.

Omi, Asif I., S. I. Sagar, M. M. H. Sajeeb, Bachir Younes, Tutku Karacolak, and Praveen Sekhar. 2023. "A New Analytically Designed UWB Microstrip Patch Antenna for Future 5G and 6G Applications." 1(1):62–63.

Pant, Rashmi, and Leeladhar Malviya. 2023. "THz Antennas Design , Developments , Challenges , and Applications : A Review." *International Journal of Communication Systems* (November 2022):1–39. doi: 10.1002/dac.5474.

Sherif A. Khaleel, Ehab K. I. Hamad, and Naser Ojaroudi Parchin. 2022. "MTM-Inspired Graphene-Based THz MIMO Antenna Configurations Using Characteristic Mode Analysis For." *Electronics* 11(2152):1–21.

Vyas, Ajay Kumar. 2019. "5G Green Communication : A Review Report."
Vyas, Narayan Krishan, and Salim Mohammad. 2020. "High Gain Antenna Design for 6G Wireless Applications." 1–10.

Wang, Cheng Xiang, Xiaohu You, Xiqi Gao, Xiuming Zhu, Zixin Li, Chuan Zhang, Haiming Wang, Yongming Huang, Yunfei Chen, Harald Haas, John S. Thompson, Erik G. Larsson, Marco Di Renzo, Wen Tong, Peiying Zhu, Xuemin Shen, H. Vincent Poor, and Lajos Hanzo. 2023. "On the Road to 6G: Visions, Requirements, Key Technologies, and Testbeds." *IEEE Communications Surveys and Tutorials* 25(2):905–74. doi: 10.1109/COMST.2023.3249835.

Wong, Kin-lu, Shao-en Hong, and Wei-yu Li. 2023. "Low-Profile Four-Port MIMO Antenna Module Based 16-Port Closely-Spaced 2 × 2 Module Array for 6G Upper Mid-Band Mobile Devices." *IEEE Access* 11(October):110796–808. doi: 10.1109/ACCESS.2023.3322730.

You, Chisang, Doochan Jung, Moonsoo Song, and Kin-lu Wong. n.d. "Advanced Coupled-Fed MIMO Antennas for Next Generation 5G Smartphones." i:11–12.

Ziegler, Volker, Harish Viswanathan, Hanu Flick, Hoffman Marco, Vilho Raisanen, and Hatonen Kimmo. 2020. "6G Architecture to Connect the Worlds." *IEEE Access* 8. doi: 10.1109/ACCESS.2020.3025032.